Smart Structures and Systems, *Vol. 19, No. 4 (2017) 341-350*
DOI: https://doi.org/10.12989/sss.2017.19.4.341

Optimum design and vibration control of a space structure with the hybrid semi-active control devices

Meng Zhan*[1], Sheliang Wang[1], Tao Yang[1], Yang Liu[1,2,3] and Binshan Yu[1]

[1]*Department of Civil Engineering, Xi'an University of Architecture and Technology, No.13 Yanta RD., Xi'an, Shaanxi 710055, PR China*
[2]*Key Laboratory of Green Building in West China, Xi'an University of Architecture and Technology, No.13 Yanta RD., Xi'an, Shaanxi 710055, PR China*
[3]*School of Civil Engineering and Geodesy,Shaanxi College of Communication Technology, No.19 Wenjing RD., Xi'an, Shaanxi 710018, PR China*

(Received June 6, 2016, Revised November 24, 2016, Accepted December 8, 2016)

Abstract. Based on the super elastic properties of the shape memory alloy (SMA) and the inverse piezoelectric effect of piezoelectric (PZT) ceramics, a kind of hybrid semi-active control device was designed and made, its mechanical properties test was done under different frequency and different voltage. The local search ability of genetic algorithm is poor, which would fall into the defect of prematurity easily. A kind of adaptive immune memory cloning algorithm(AIMCA) was proposed based on the simulation of clone selection and immune memory process. It can adjust the mutation probability and clone scale adaptively through the way of introducing memory cell and antibody incentive degrees. And performance indicator based on the modal controllable degree was taken as antigen-antibody affinity function, the optimization analysis of damper layout in a space truss structure was done. The structural seismic response was analyzed by applying the neural network prediction model and T-S fuzzy logic. Results show that SMA and PZT friction composite damper has a good energy dissipation capacity and stable performance, the bigger voltage, the better energy dissipation ability. Compared with genetic algorithm, the adaptive immune memory clone algorithm overcomes the problem of prematurity effectively. Besides, it has stronger global searching ability, better population diversity and faster convergence speed, makes the damper has a better arrangement position in structural dampers optimization leading to the better damping effect.

Keywords: SMA and PZT; composite damper; hybrid semi-active control; mechanical test; memory unit; antibody incentive degrees

1. Introduction

With the development of the intelligent materials, the vibration control device made by intelligent materials is gradually used in civil engineering structural vibration reduction domain. SMA (Shape Memory Alloy) is a kind of intelligent metal perception and drive materials with excellent properties which not only has shape memory and super-elasticity two unique performances, but also has the advantages of high damping, fatigue resistance and corrosion resistance. it has been widely used in the field of civil engineering (El-Attar *et al*. 2008, Contreras *et al*. 2014, Zhou *et al*. 2015 and Xu *et al*. 2015). PZT (piezoelectric) is a kind of functional material with positive and inverse piezoelectric effect, and piezoelectric friction damper made by inverse piezoelectric effect has stable performance like the friction energy dissipater, has the characteristics of response speed like the piezoelectric material, and at the same time has the advantages of semi-active controller's small input energy. At present, a variety of piezoelectric friction dampers have been proposed for (Chen and Chen 2004, Ozbulut *et al*. 2010, Etedali *et al*. 2013) vibration control. However, in order to make the deformation of the piezoelectric ceramic actuator has a better constraint, it often needs to implement a large pressure on piezoelectric friction damper. For example, herringbone piezoelectric friction damper, designed by Zhao and Li (2011), needs a pressure of 2000N, but the maximum output of piezoelectric ceramic actuator is only 400 N. It is more like a passive friction damper because the adjustable control range is so small; Shaft piezoelectric friction damper, designed by Zhan *et al*. (2014), has a small pressure, but the maximum output of piezoelectric ceramic actuator is also small. Neither of them has effective damping effect. Some scholars put the SMA and PZT materials together for structural vibration control, and the current researches mainly focus on the active/passive hybrid control of beam with Weak vibration. For example, Choi *et al*. (1998), Sun *et al*. (1999) and Yuvaraja and Senthilkumar (2013) discussed a hybrid control of beams using SMA and PZT materials and the results show that hybrid control is better than a single control. Nevertheless, the composite dampers with SMA and PZT have few researches. Dai (2012) designed a SMA and piezoelectric composite friction damper, and applied it to base earthquake isolation structure and got a good effect. But its size is larger. SMA works relying on sliding of PZT friction damper. They both must work at the same time, so it still cannot conquer the

*Corresponding author, Ph.D.
E-mail: zhanyi313@163.com

ISSN: 1738-1584 (Print), 1738-1991 (Online)

disadvantage of piezoelectric friction damper. Here, a damper is designed by author in which SMA wires and piezoelectric friction damper can work in turn. When small earthquakes happen, SMA wires work alone, when great earthquakes happen, SMA wires work first, and then SMA wires and piezoelectric friction damper work at the same time. The SMA and PZT friction composite damper can real-time adjusting control force.

Dampers' damping effect is mainly decided into three aspects: damper performance, installation position and the number. Therefore, in order to get a better damping and economical effect, it needs to optimize the structure to determine the optimal location and number of dampers. Genetic algorithm is a kind of evolutionary algorithms. It finds the optimal solution by imitating the nature selection and heritage, and it has been widely applied to the optimization of damper (Yan and Zhou 2006, Ok *et al*. 2008). But the local search of genetic algorithm is poor, and search efficiency is low in late evolution. It has not been able to solve the problem with large amount of complicated calculations in practice, and astringes easily to the local optimal solution, producing prematurity phenomenon. Adaptive immune memory cloning algorithm (AIMCA) is a new kind of artificial immune algorithm, which simulates self-regulation, memory, learning and adaptive mechanism of the immune system, realizing the combination of global optimization and local optimization. Through the calculation of antibody-antigen affinity and antibody-antibody affinity, it promotes and inhibits the production of antibodies, and adjusts the clone scale of antibody group and memory unit adaptively. The algorithm has strong global search ability, good population diversity and convergence speed. It can effectively solve the problem of prematurity. In this paper, SMA and PZT friction composite damper was designed and made. Its mechanical properties were tested under different frequency and different voltage. Then the damper is applied to the space structure, using genetic algorithm and AIMCA to explore the advantages and feasibility of AIMCA for optimization analysis.

2. SMA and PZT friction composite damper

2.1 structural design

The flat section and front elevation of SMA and PZT friction composite damper are shown in Figs. 1(a)-(b). On the left and right sides of damper box, there are two hex flange toothed bolts with gasket to fix SMA wire 1 and 2 respectively. There are two small holes in front and back sides. A sliding block is put in the damper box and the SMA wire 1 and 2 have a roundabout via its each side. PZT ceramic actuators are located into four round holes and each sidewall has a small hole. There is a gasket on the upper and lower side of each PZT ceramic actuator. Left baffle which slides in left sliding groove was set up on the left side of the sliding block and right baffle which slides in right sliding groove was set up to the right side. On the left baffle, there are two hex flange toothed bolts and there are two small holes on right baffle. SMA wire 1 which gets through the left baffle and sliding block is fixed on the left side of the damper using hex flange toothed bolts. SMA wire 2 which gets through the right baffle and sliding block is fixed on the right side of the damper. SMA wire 3 which gets through the sliding block and right baffle is fixed on the left baffle. Push-pull rod which gets through the left side of damper box, left baffle and sliding block is brought into contact with right baffle, but is not fixed. There is a left baffle ring at the contact site with left baffle. And there is a right baffle ring at the contact site with right baffle. The connecting rod on the right side of damper can be fixed with structure by bolts. The pre-pressure can be changed by adjusting the socket head cap screw on the lid of the damper.

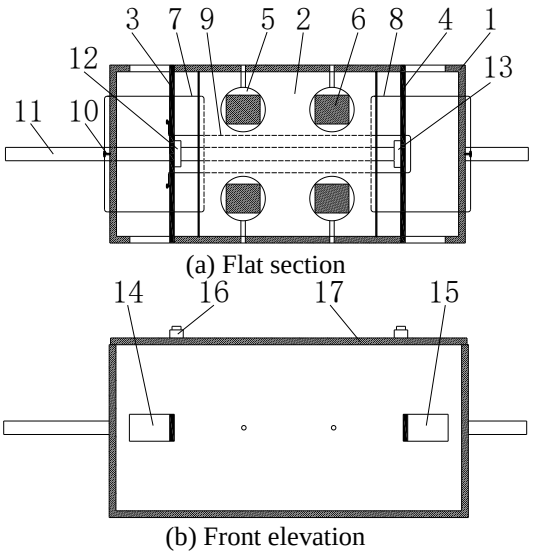

Fig. 1 Schematic diagram of PTZ and SMA friction damper

In the figures above: 1.damper box; 2. sliding block; 3. Left baffle; 4. right baffle; 5.PZT ceramic; 6. gasket; 7.SMA wire 1; 8.SMA wire 2; 9.SMA wire 3; 10. hex flange toothed bolts; 11. push-pull rod; 12. left baffle ring; 13. right baffle ring; 14. left groove; 15. right groove; 16. Preloaded bolt; 17.damper lid

2.2 working principle

As the push-pull rod is pulled into the left along axis direction, the right baffle gets stuck to the left endpoint of the right groove motionlessly at this moment. When the left baffle moves to the left under the action of left blocking ring, the SMA wire 3 begins to dissipate the energy passively. When the push-pull rod receives greater force, the left baffle continues to slide to the left. When the right blocking ring moves to the right endpoint of sliding block, the sliding block and the left baffle begin to move to the left together. The SMA wire 2 is tensed at this moment meanwhile the SMA wire 2, 3 and sliding block all consume energy. The output of the PZT actuator can be changed by applying different voltages.

As the push-pull rod was pulled into the right along axis direction, the left baffle gets stuck to the right end of the left groove motionlessly at this moment. And the right blocking

ring begins to resist the right baffle and moves to the right. The SMA wire 3 begins to dissipate energy passively. When left blocking ring moves to the left end of sliding block, the sliding block and the right baffle begin to move to the right together, and the SMA wire 1 is tensed at this moment. The SMA wire 1, 3 and sliding block all consume energy and the output of PZT actuator can be changed by applying different voltages.

2.3 mechanical test

Fig. 2 displays the physical model of SMA and PZT friction composite damper. The diameter of SMA wire is 0.7 mm. The numbers of SMA wire 1 and 2 are both 4 and the length is 100 mm, and the maximum elongation is 7 mm. The number of SMA wire 3 is 2 and the length is 175 mm, the work displacement alone is 5 mm, and the maximum elongation is 12 mm which is the same as the maximum displacement of damper. The size of rectangular PZT ceramic actuator is 10 mm×10 mm×36 mm and the maximum elongation is 40um. The maximum input voltage is 150V and the maximum output pressure is 3.6 kN in theory when applied preloading is 1.5 kN. All parts of the damper are made of aluminum alloy and the initial friction is 0.2 kN.

The test was implemented using HT9711 material testing machine, as shown in Fig. 3, In the test the displacement control was used. Frequency of triangle wave for loading-unloading was 0.05 Hz, 0.1 Hz, 0.2 Hz and 0.3 Hz, loading amplitude was 5 mm (SMA wire 3 working alone), 9 mm and 12 mm, Voltage is provided by dc regulated power supply, for 0V, 40V, 80V and 120V. Before the test, the damper in the frequency of 0.1 Hz, voltage of 0V, the maximal displacement of 12 mm was in tension and compression cycle was 30 times, which ensured the mechanical properties of SMA wires to achieve stable. There are two tensions and compression circles for each working condition.

Fig. 4 shows output force - displacement curve for different frequency when SMA wire 3 works alone. Figs. 5(a)-(b) and 6(a)-(b) show output force - displacement curves for different frequency at 40V and 120V. It can be seen that the damper has good energy dissipation and stable performance, its performance has little relationship with frequency. Figs. 7(a) and (b) show output force - displacement curve for different voltage at 0.1 Hz. It can be observed that, with the increase of input voltage, the area of hysteresis loop gradually increasing, and the energy dissipation ability improves. When voltage increases from 0V to 120V, the friction force has an increment of 0.4 kN, which is obviously better than the dampers designed by Li and Zhu.

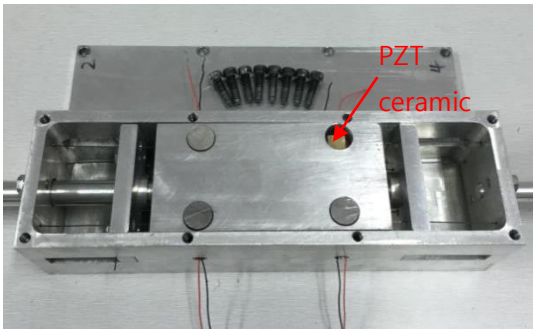

Fig. 2 Damper model

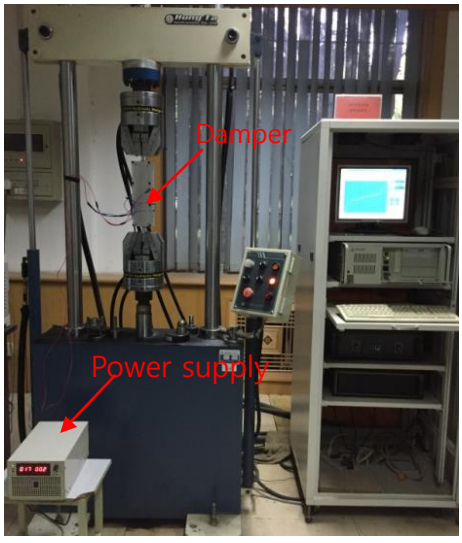

Fig. 3 Test device

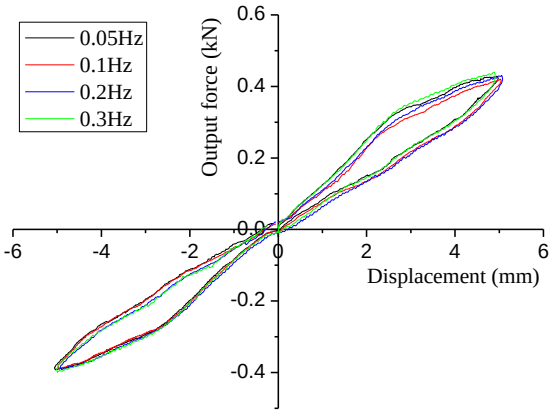

Fig. 4 Output force - displacement curve when SMA wire 3 works alone

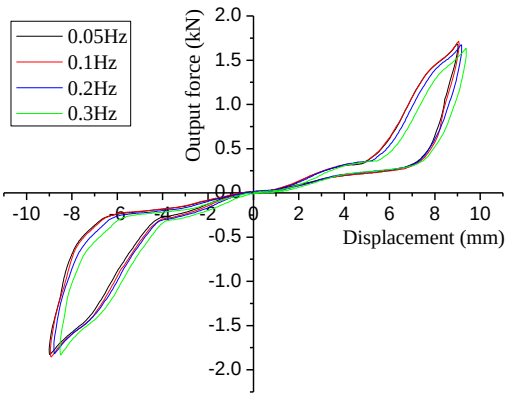

(a) 9 mm

Fig. 5 Output force - displacement curve for different frequency at 40V

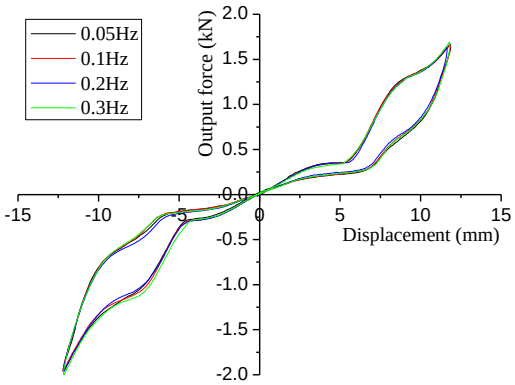

(b) 12 mm

Fig. 5 Continued

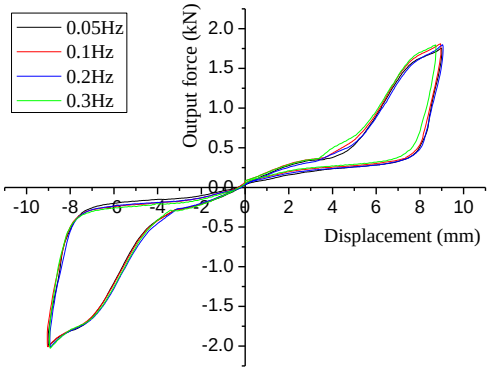

(a) 9 mm

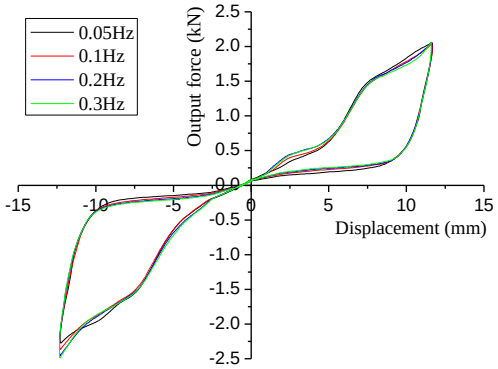

(b) 12 mm

Fig. 6 Output force - displacement curve for different frequency at 120V

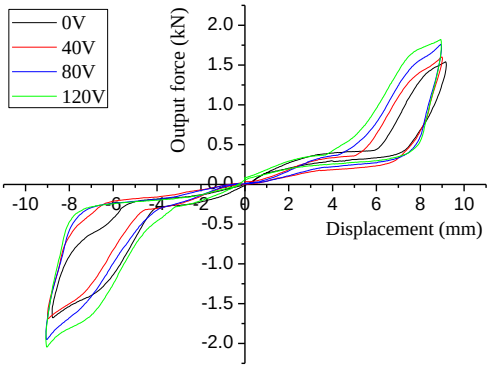

(a) 9 mm

Fig. 7 Output force - displacement curve for different voltage at 0.1 Hz

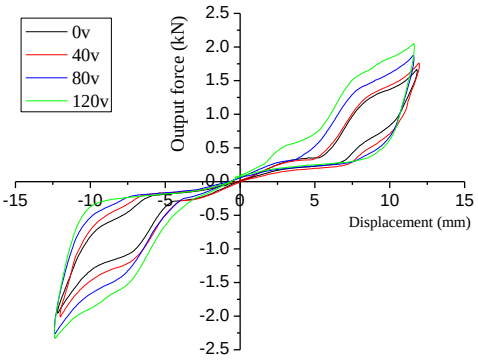

(b) 12 mm

Fig. 7 Continued

3. performance indicators based on modal controllable degree

Controlled structural dynamic equation can be represented as

$$[M]\{\ddot{X}\} + [C]\{\dot{X}\} + [K]\{X\} = [D_S]\{F\} + [B_S]\{U_C\} \quad (1)$$

Where $[M]$、$[C]$、$[K] \in R^{n\times n}$ denote the quality, damping, and stiffness matrices of the controlled structure, $\{\ddot{X}\}$、$\{\dot{X}\}$、$\{X\} \in R^{n\times 1}$ denote the acceleration, velocity and displacement vector of structure, $\{F\} \in R^{r\times 1}$ is the earthquake force vector, $[D_S] \in R^{n\times r}$ is the earthquake location matrix, $\{U_C\} \in R^{P\times 1}$ is vector of control force, $[B_S] \in R^{n\times P}$ is dampers' control position matrix, "n" is the number of structural degrees of freedom, "p" is the number of dampers.

Using the canonical mode (Cho *et al*. 2005) to decouple the Eq. (1), $\{X\}$ is given as

$$\{X\} = \sum_{r=1}^{n}\{\phi_r\}\, q_r \quad (2)$$

Without considering the earthquake force, put the Eq. (2) into the Eq. (1)

$$\sum_{r=1}^{n}[M]\{\phi_r\}\ddot{q}_r + \sum_{r=1}^{n}[C]\{\phi_r\}\dot{q}_r + \sum_{r=1}^{n}[K]\{\phi_r\}q_r = [B_S]\{U_C\} \quad (3)$$

Both sides of the Eq. (3) times $\{\phi_i\}^{\mathrm{T}}$

$$\sum_{r=1}^{n}\{\phi_i\}^{\mathrm{T}}[M]\{\phi_r\}\,\ddot{q}_r + \sum_{r=1}^{n}\{\phi_i\}^{\mathrm{T}}[C]\{\phi_r\}\,\dot{q}_r + \sum_{r=1}^{n}\{\phi_i\}^{\mathrm{T}}[K]\{\phi_r\}q_r = \{\phi_i\}^{\mathrm{T}}[B_S]\{U_C\} \quad (4)$$

Due to the vibration mode of orthogonal sex, the Eq. (4) can be simplified as

$$\{\phi_i\}^{\mathrm{T}}[M]\{\phi_i\}\ddot{q}_i + \{\phi_i\}^{\mathrm{T}}[C]\{\phi_i\}\dot{q}_i + \{\phi_i\}^{\mathrm{T}}[K]\{\phi_i\}q_i = \{\phi_i\}^{\mathrm{T}}[B_S]\{U_C\} \quad (5)$$

Both sides of the Eq. (5) divide by $M_i = \{\phi_i\}^{\mathrm{T}}[M]\{\phi_i\}$, then the "i" th step modal equation can be obtained as

$$\ddot{q}_i + 2\xi_i\omega_i\dot{q}_i + \omega_i^2 q_i = \{B_i\}\{U_c\} \tag{6}$$

where q_i is the "i" th step modal coordinates, ω_i is the "i" th step natural frequency of vibration, ξ_i is the "i" th step modal damping ratio, $\{\phi_i\} \in R^{n\times 1}$ is the "i" th mode vector. $\{B_i\} = \{\phi_i\}^{\mathrm{T}}[D]$, $[D] = [B_S]/M_i = [B_S]/\{\phi_i\}^{\mathrm{T}}[M]\{\phi_i\}$

Singular value decomposition to $\{B_i\}$

$$\{B_i\} = U_i\{S_i\}[V_i]^{\mathrm{T}} \tag{7}$$

Where $\{B_i\} \in R^{1\times P}$, $\{U_i\} \in R^{1\times 1}$, $\{S_i\} \in R^{1\times P}$, $\{V_i\} \in R^{P\times P}$, ${U_i}^{\mathrm{T}}U_i = 1$, $[V_i]^{\mathrm{T}}[V_i] = \mathrm{I}$.

If mode q_i is controlled, the rank of $\{B_i\}$ is equal to 1. The singular value vector $\{S_i\}$ of $\{B_i\}$ can be expressed as

$$\{S_i\} = \{0 \cdots \sigma_i \cdots 0\} \tag{8}$$

And because $\{U_i\} \in R^{1\times 1}$, ${U_i}^{\mathrm{T}}U_i = 1$, so $U_i^{\mathrm{T}} = U_i = 1$.

Put $\{B_i\} = \{\phi_i\}^{\mathrm{T}}[D]$ and $U_i^{\mathrm{T}} = U_i = 1$ into the Eq. (7)

$$\{B_i\} = \{\phi_i\}^{\mathrm{T}}[D] = \{S_i\}[V_i]^{\mathrm{T}} \tag{9}$$

By the same token, a set of modal coordinates $\{p\} = \{p_1, \cdots, p_i, \cdots, p_n\}$ and the Eq. (9) are put into the Eq. (6), regardless of the earthquake force, the Eq. (10) is got as

$$\ddot{p}_i + 2\xi_i\omega_i\dot{p}_i + \omega_i^2 p_i = \{S_i\}[V_i]^{\mathrm{T}}\{U_c\} \tag{10}$$

Let $\{\overline{U}_c\} = [V_i]^{\mathrm{T}}\{U_c\}$, and put it into the Eq. (10)

$$\ddot{p}_i + 2\xi_i\omega_i\dot{p}_i + \omega_i^2 p_i = \{S_i\}\{\overline{U}_c\} = \{0 \cdots \sigma_i \cdots 0\}\{\overline{U}_c\} \tag{11}$$

Contrast the Eq. (10) and the Eq. (11), because of $[V_i]^{\mathrm{T}}[V_i] = \mathrm{I}$, so $[V_i][V_i]^{\mathrm{T}} = \mathrm{I}$, then

$$\{\overline{U}_c\}^{\mathrm{T}}\{\overline{U}_c\} = \{U_c\}^{\mathrm{T}}[V_i][V_i]^{\mathrm{T}}\{U_c\} = \{U_c\}^{\mathrm{T}}\{U_c\} \tag{12}$$

So we can regard $\{U_c\}$ and $\{\overline{U}_c\}$ are the same on the energy consumption. Therefore, the controllable degree of p_i can be measured by the size of σ_i in the vector $\{S_i\}$. the greater the σ_i, the control effect to p_i is greater under the same energy level. Performance indicators based on modal controllable degree can be defined as

$$\mathrm{J} = \sum_{i=1}^{n}\gamma_i\,\sigma_i^2 \tag{13}$$

Where γ_i reflects importance of the "i" th controlled modal. Because the control objects are mainly the earthquake response of space structures, so γ_i can be got for the corresponding value to w_i which is at the earthquake influence coefficient curve. The greater the performance index *J*, the more reasonable the layout of SMA and PZT friction composite damper, the better the structural control effect (Liu *et al*. 1994).

4. Adaptive immune memory cloning algorithm

Property index J is considered as target function and the problem of damper optimization in civil engineering can be described as follow:

Find：$[B_S]$；Max: J；St: $[B_S] \in [B_S{}^*]$

4.1 Construction of affinity function

Target function is considered as antibody-antigen affinity function and the affinity between antibodies is taken into consideration at the same time. Affinity between antibodies can be reflected by the Eq. (14) (Liu *et al*. 2005)

$$D_{ij} = \|\alpha_i - \alpha_j\| = \sqrt{\sum_{l=1}^{L}(\alpha_{il} - \alpha_{jl})^2} \tag{14}$$

$$(i, j = 1,2 \cdots, n)$$

Where $\|\cdot\|$ is any norm, Hamming distance is used for binary system, Euler distance is used for real number encoding. "n" is the magnitude of population. α_i , α_j is two antibodies in antibody cluster and "L" is coding length. $D = (D_{ij})_{n\times n}$ is a symmetric matrix and can reflect the diversity of population. The similarity level and the affinity between antibodies become smaller when D_{ij} become larger.

Defining the number "i" th density of antibody

$$\rho_i = \exp\left(-\sum_{j=1}^{n} D_{ij}\right) \tag{15}$$

Obviously, as the density of the antibody decreases, the restraint between antibodies gets weaker. As the level of similarity between antibodies gets smaller, the scale of clone gets larger.

4.2 Calculation steps

Step 1 Assuming that K=0, Initial antibody cluster $A(0) = \{a_1(0), a_2(0), \cdots, a_n(0)\}$ is generated randomly when the mutation probability p_m and clone scale N are given.

Step 2 Calculating the magnitude of antibody-antigen affinity $f(A(0))$.

$$f(A(0)) = \{f(a_1(0)), f(a_2(0)), \cdots, f(a_n(0))\}$$

Step 3 According to the magnitude of antibody-antigen affinity, antibody cluster $A(k)$ is sorted from big to small. Top "t" antibodies are chosen as memory units $A_m(k) = \{a_1(k), a_2(k), \cdots, a_t(k)\}$ and others are considered as normal antibody units $A_r(k) = \{a_{t+1}(k), a_{t+2}(k), \cdots, a_n(k)\}$. The magnitude of "t" is determined by the affinity between antibodies and it is indicated as follows

$$t = \mathrm{floor}[n \times (s_c + \theta)] \tag{16}$$

Where floor( ) is rounding down function, s_c is the constant which is designed to guarantee the basic magnitude of memory unit.

Step 4 Adjusting mutation probability. Firstly, mutation probability of each antibody is calculated.

$$p_m^i(k) = p_m + \left[1 + \exp\left(L \cdot \frac{f(a_i(k))}{\sum_{i=1}^{n} f(a_i(k))}\right)\right]^{-1} \tag{17}$$

Memory unit is a better individual, the mutation

probability should be as small as possible, and normal antibody unit should implement the large variation. so memory unit and normal antibody unit probability threshold can be given as p_m^M and p_m^R, $p_m^i(k)$ can be amended as

$$p_m^i(k) = \begin{cases} p_m^m, & p_m^i(k) \geq p_m^m, \quad i = 1,2,\cdots,t \\ p_m^r, & p_m^i(k) \leq p_m^r, \quad i = t+1, t+2, \cdots, n \end{cases} \tag{18}$$

Step 5 New antibody cluster is obtained by cloning and cloning mutations.

1) Clone T_c^c. The antibody cluster after clone

$$B(k) = \{T_c^c(a_1(k)), T_c^c(a_2(k)), \cdots, T_c^c(a_n(k))\}$$

Where $T_c^c(a_i(k)) = I_i \times a_1(k)$ is clone of antibody a_i, $I_i = \text{ones}(1, n_i)$ is n_i dimensional row vector.

Antibody excitation extent λ_i is introduced

$$\lambda_i = f(a_i(k)) \cdot \exp(-\rho_i) \tag{19}$$

n_i is determined by the formula

$$n_i = \text{ceil}\left(N \times \frac{\lambda_i}{\sum_{i=1}^n \lambda_i}\right) \tag{20}$$

Where $N = \sum_{i=1}^n n_i$ is total scale of clone antibody, ceil( ) is rounding function.

It is observed that the antibody density ρ_i and antibody-antigen affinity $f(a_i(k))$ self-adaptive adjustment can be used to show the antibody scale. When the density of antibody is small and antigen affinity is big, excitation extent λ_i becomes bigger and so do the clone scale. This not only keeps better individuals but also increases the population diversity.

2) Clone mutation T_c^m. If it is binary coding, the site mutation is used; If it is real number encoding, the Gaussian mutation is used, and the antibody has mutation by using following formula

$$a_i = a_i(1 + \delta \times N(0,1)) \tag{21}$$

Where δ is decreasing variable between 0 and 1, $N(0,1)$ obeys the Gaussian distribution which mean value is 0 and variance is 1. As is shown, antibody after mutation antibody increases the decreasing type of Gaussian distribution stochastic disturbance $a_i \times \delta \times N(0,1)$ on the basis of original antibody. This can increase the diversity of population and be beneficial for jumping out of locally extreme point and doing global search. Meanwhile, it can improve the speed of convergence. The new antibody cluster $C(k) = T_c^m(B(k))$ can be obtained after clone mutation.

Step 6 Calculating the antibody -antigen affinity $f(C(k))$.

Step 7 Clone selection T_c^s. For $\forall i = 1,2\cdots,n$, if the antibody "b" after mutation satisfy

$$f(\alpha_i) < f(b), \alpha_i \in A \tag{22}$$

"b" can be used to replace the original antibody . Furthermore, the antibody cluster is renewed and the information is exchanged. After completing the clone selection, the next generation of antibody cluster $A(k+1) = T_c^s(C(k))$ can be obtained and maximum evolution generation is considered as the end condition of the arithmetic.

5. Optimum and control of the space structure with dampers

5.1 Spatial member structure model

In order to clarify the advantages of AIMCA over the standard genetic algorithm (SGA) of keeping optimum individual in dampers optimization, a three-story spatial structure is used as the object of the study and shown in Fig. 8. The structure has 2 spans which are 1m along the X axis and 1 span which is 1.2 m along the Y axis. The height of each story is 1m and the bottom is constrained by 6 supports. It has 24 joints and 39 members. The sizes of all the structural members are the same as follows: external diameter is 16 mm, wall thickness of Q235 circular steel tube is 2 mm, elasticity modulus is 206GPa, Poisson's ratio is 0.3, density is 7.85×10^3 Kg/m^3. Every member has solid joints. 2Kg Steel balls are arranged at every joint to simulate loads and make it more convenient to connect. Also assuming that all mass concentrated on the joints of every floor. Because the control effect of SMA and PZT friction composite damper is mainly related to the relative displacement of both ends, dampers are arranged along the direction of structural inter-lamination diagonal brace. Possible locations are 18 and shown by red dotted lines as follows.

5.2 Optimized results and analysis

5.2.1 Parameters of optimization algorithms

Initial population of SGA is 50 and crossover probability is 0.9. The mutation probability is 0.01 and the rate of generating new individual is 90%. The initial antibody population of AIMCA is 30 and the mutation probability p_m is 0.1, probability threshold value of

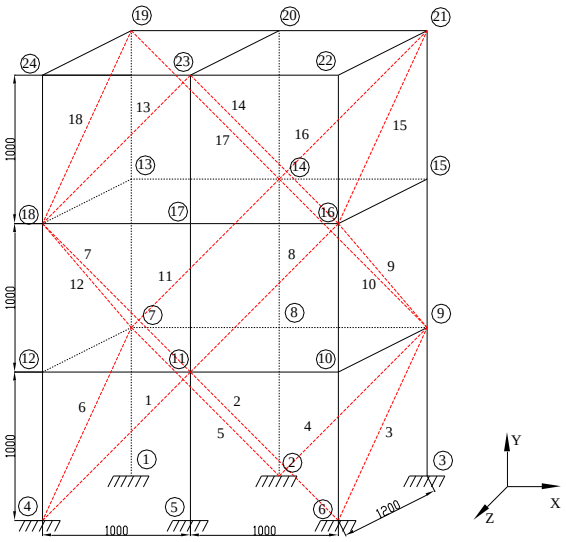

Fig. 8 Space model structure diagram

normal antibody unit p_m^r is 0.1, probability threshold value of memory unit p_m^m is 0.01, quantity of memory unit s_c is 5.

The clone scale is 50 and run 5 times alone. The average value is considered as simulation result and real number coding is used.

5.2.2 results and analysis

Among 5 times running, AIMCA can search the global optimum value every time; however, SGA has a big fluctuation for the value of every running, and global optimum value can be hardly found. The performance indexes (see Table 1) of different quantity of dampers at 50 termination generations are shown in Fig. 9. It can be seen that when the quantity of dampers increases, the performance index value increases gradually and damping effect on the structure increases gradually too. The performance indicator for 4 dampers has been close to 20, when the quantity of dampers is over four, the increasing rate decreases rapidly. When the quantity of dampers is over 14, the performance index value hardly changes for the reason that the remainder optimization space of these two arithmetic is small, the performance indicator with all dampers is only 28.5, so 4 dampers can be considered a relatively economic and appropriate quantity. Compared with the SGA, the performance index value of AIMCA is bigger and has a better optimization.

Figs. 10(a)-(b) and 11(a)-(b) display the convergence processes of mean values and optimal values for every generation in the condition that the quantity of the dampers is 4 and 8 respectively. From Figs. 10(a)-(b), it can be seen that mean values of each generation of SGA gradually increases in "steps" shape, but convergence curve of AIMCA is a horizontal wavy lines which has larger volatility in the whole process of evolution. These show that the population renewal ability of SGA is poor, and species of AIMCA got effective updates with the increasing of evolution algebra and AIMCA has maintained good population diversity. It is observed from Figs. 11(a)-(b) that AIMCA converges to the global optimal solution before the 40 generation, however, SGA converges to the locally optimal value after 100 generation. This shows that AIMCA converges faster and has a better stability than SGA . It overcomes the problem of precocity and efficiently avoids the situation that it falls into locally optimum solution.

Table 1 The performance indexes of different number of dampers

Damper quantities	0	2	4	6	8	10	12	14	16
SGA	0	12.96	17.63	19.82	22.69	24.22	25.89	27.67	28.39
AIMCA	0	13.13	19.24	21.57	23.52	25.26	26.88	27.72	28.49

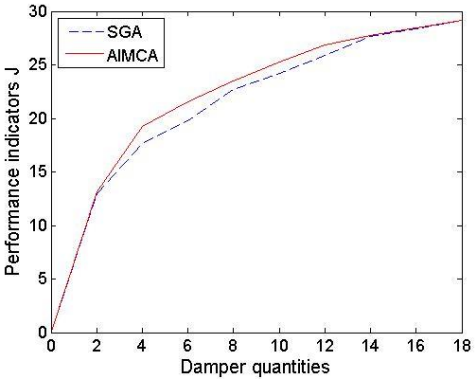

Fig. 9 Performance index of different quantity of dampers

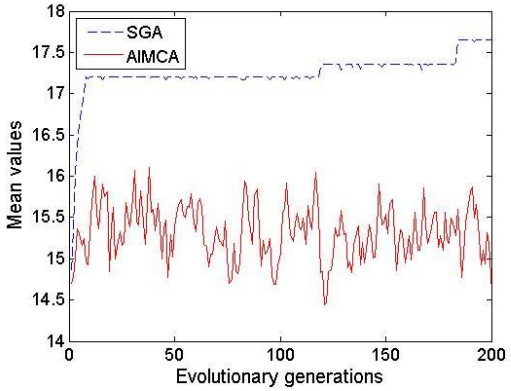

(a)4 dampers

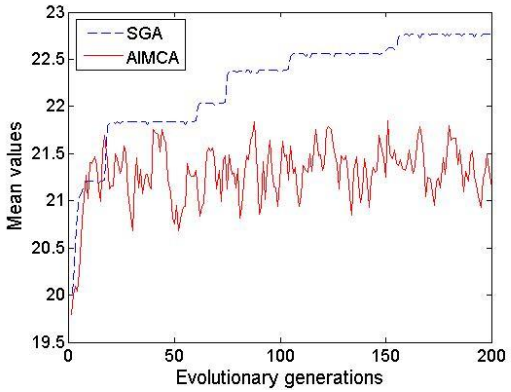

(b)8 dampers

Fig. 10 The convergence process of mean values of every generation

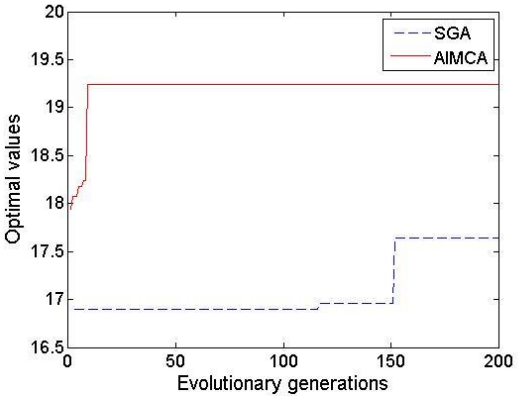

(a)4 dampers

Fig. 11 The convergence process of optimal values of every generation

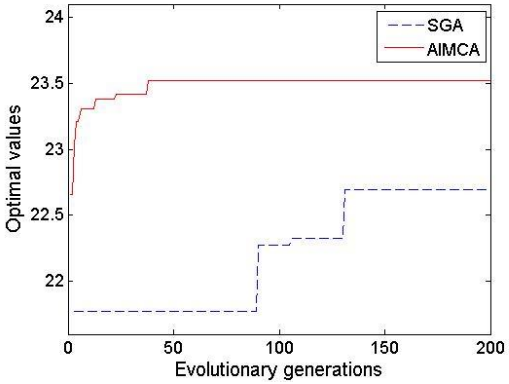

(b)8 dampers

Fig. 11 Continued

Table 2 Location optimization result of 4 dampers

Optimization algorithms	Location optimization results	Objective function values
SGA	1,9,15,16	17.63
AIMCA	4,9,10,15	19.24

5.3 Seismic response analysis

The El Centro wave and Taft wave both have 20s time of duration, 0.02s interval and 400 gal peak acceleration amplitude is chosen in the seismic excitation and is loaded uniaxially along the *x* axis. Four dampers are chosen and arranged to control the earthquake response and optimal placement after the SGA and AIMCA optimizing is shown in Table 2.

5.3.1 Control strategy

Based on the BP neural network and T-S fuzzy controller, the structural vibration control is realized. Firstly, the neural network constitutive model of the damper is built according to the data of the experiment. The reaction speed of the structure is regarded as the input of the fuzzy controller and the value of the voltage is regarded as the output. Then the value of voltage, speed sign function and displacement are regarded as three input of the neural network. The controlling force is the output. The semi-active controlling force can be got as follows:

(1) BP neural network constitutive model of the damper BP network of three layers is chosen. The value of voltage *U*, speed sign function sign(*v*) and displacement *x* are regarded as neuron input. And the controlling force *f* is regarded as output. The quantity of implicit strata, which is determined by using estimating method is 12. Therefore, the topological structure of the network is 3-12-1.

Constitutive model of the damper is chosen to control the vibration of the structure when it is 12 mm. And the working condition is 16. Four groups experiment data when the voltages are 0V/40V/80V/120V and the frequency is 0.1 HZ are regarded as testing data. And other twelve groups data are regarded as training data. The procedure of training is shown in Fig. 12. The comparing picture between prediction curve and experiment curve when the voltages are 40V and 120V is shown in Figs. 13(a)-(b). As is shown in the picture, the prediction curve and the experiment curve of the neural network are anastomotic. Comparing with the prediction result of 120V, the result is worse when the voltage is 40V because the data of 40V has a big fluctuation.

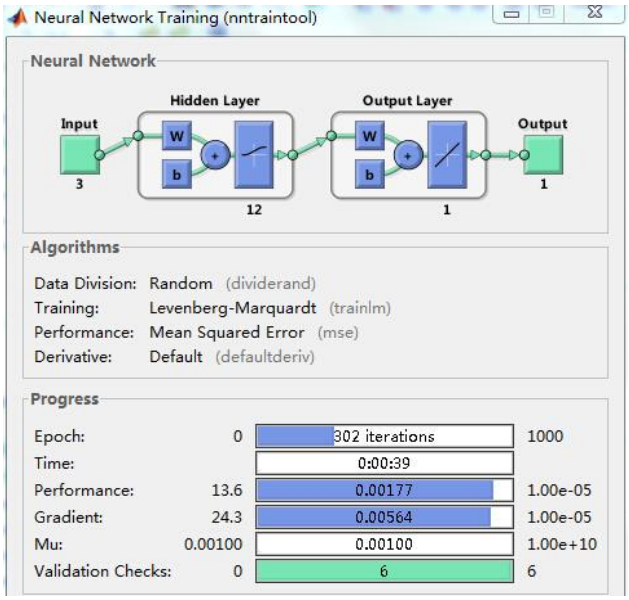

Fig. 12 Training process

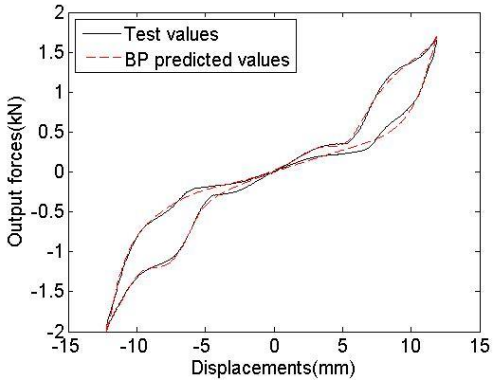

(a) 40v

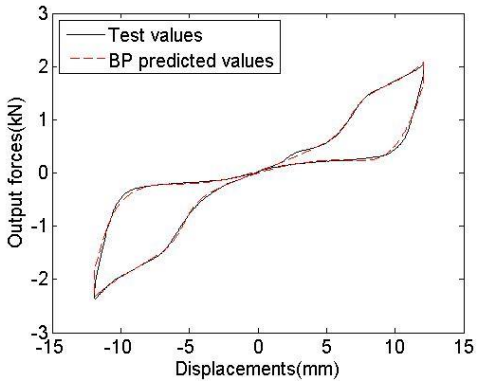

(b) 80v

Fig. 13 Contrast curve between BP network prediction and test

(1) T-S fuzzy control

The relevant speed of the two end of the damper is regarded as the input of fuzzy control. The boundary of the domain of discourse is the absolute maximum of the relevant speed without controlling. The voltage is regarded as the output. And the fuzzy domain of discourse of the input variable is [-2, 2]. Six fuzzy subset are chosen. And the corresponding fuzzy language is $M_{f1}, M_{f2}, M_{f3}, M_{f4}, M_{f5}, M_{f6}$. The Gaussian distribution function is chosen as the membership function. Zero-order T-S fuzzy reasoning is used. The "i"th fuzzy control rule R_i can be expressed as, R_i: if v is M_{fi}, then $y_i = k_i (i = 1,2,\cdots,6)$, k_i is indicated as follows

$$k_i = \begin{cases} 0 & i = 1,2,3 \\ 120\text{V} & i = 4,5,6 \end{cases} \tag{23}$$

Assuming that some input variable of the speed activate j fuzzy controlling regulations $(j \le 6)$. So the output U_{fc} of the fuzzy system is weighted average of j regulations output.

$$U_{fc} = \sum_{i=1}^{j} \alpha_i y_i / \sum_{i=1}^{j} \alpha_i \tag{24}$$

Where α_i is the membership degree of the "i"th fuzzy control rule.

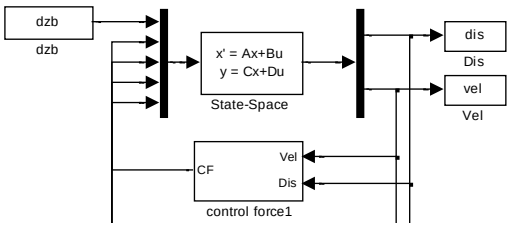

(a) Main simulation model

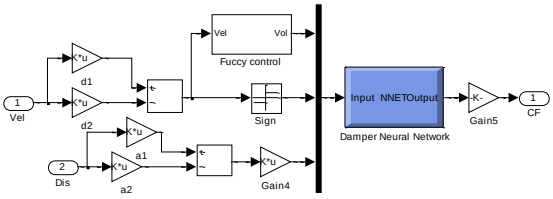

(b) Simulation model of damper's control force

Fig. 14 Vibration control simulation of space structure with the composite dampers

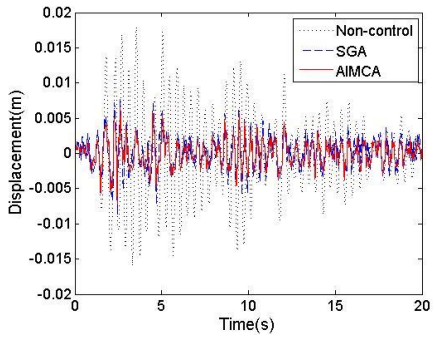

(a) displacement response

Fig. 15 Dynamic response time-history curve at El Centro wave

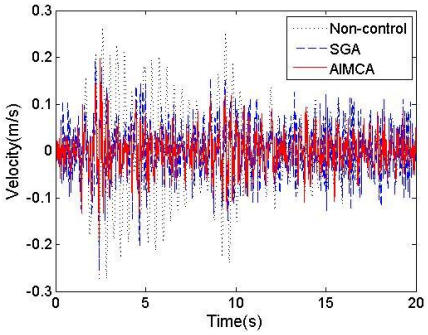

(b)velocity response

Fig. 15 Continued

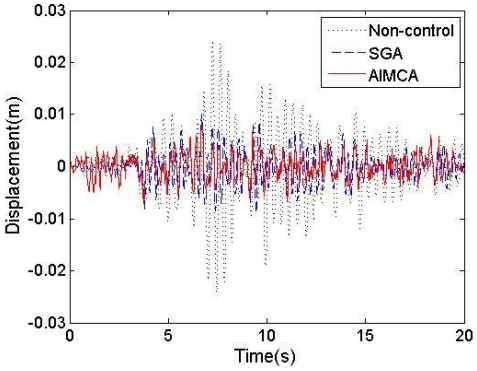

(a) displacement response

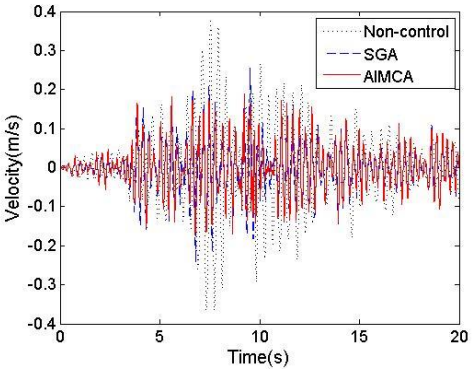

(b)velocity response

Fig. 16 Dynamic response time-history curve at Taft wave

5.3.2 Simulation models and results

Vibration control of space structure with the developed dampers was carried out via MATLAB/Simulink, and the simulation model is shown in Figs. 14(a)-(b). Figs. 15(a)-(b) and 16(a)-(b) show several conditions of displacement and acceleration time curve for joint 12 at El Centro and Taft waves: no control, optimized by SGA and AIMCA. It is observed that damper arrangement of AIMCA has a better effect on decreasing the seismic peak response of the structure than the damper arrangement of SGA.

6. Conclusions

In our work, a hybrid semi-active control device using

SMA and PZT materials was designed and made, its mechanical properties were tested. Optimum design and vibration control of a space structure with the dampers was discussed. The primary conclusions inferred from the results can be summarized as follows:

- The SMA and PZT friction composite damper have stable performance and good energy dissipation ability, can make timely adjustment of control force according to the size of voltage. When facing small vibration, the SMA wires work alone and the energy is passively consumed. When facing big vibration, the SMA and PZT friction composite damper work and consume energy together . The problem that normal piezoelectric friction damper starts difficultly is avoided when it is faced with small vibration and the supply of huge control force is guaranteed when faced with big vibration.
- According to the affinity between antibodies and the magnitude of affinity, what is done is the adaptive control for the clone scale of antibody cluster.. Meanwhile inbreeding is avoided and the diversity of antibody cluster is guaranteed. By using different mutation strategies for memory unit and normal antibody unit, the maturity of antibody affinity is accelerated and the speed of convergence is improved.
- Global searching ability of AIMCA arithmetic is very powerful and the speed of convergence is fast, meanwhile the robustness is good. The problem that the genetic variation method easily get into local convergence and the precocity shows up is avoided efficiently. The results of complex problem such as multimodal function optimization, damper optimization and so on are good.
- Based on T-S fuzzy logic and BP neural network prediction model, the structural dynamic response analysis was discussed, and better layout of damper for AIMCA and more efficient decrease for structural seismic peak reflection can be obtained .

Acknowledgments

This research was financially sponsored by the National Natural Science Foundation of China (No. 51678480), the Shaanxi province innovation projects of science and technology (No. 2013SZS01-Z02,-K01), the Shaanxi province natural science foundation project (2012JQ7018), the Key Laboratory of Green Building in West China (No. LSKF201707) and the basic research project of Ministry of Communications (No. 2015319G02190).

References

Chen, C.Q. and Chen, G.D. (2004), "Shake table tests o f a quarter-scale three-story building model with piezoelectric friction dampers", *Struct. Control Hlth. Monit.*, **11**(4), 239-257.

Cho, S.W., Kim, B.W. and Jung, H.J. (2005), "Implementation of modal control for seismically excited structures using magnetorheological dampers", *J. Eng. Mech.*, **131**(2), 177-184.

Choi, S.B., Park, Y.K. and Fukuda, T. (1998), "Proof-of-concept investigation on active vibration control of hybrid smart structures", *Mechatronics*, **8**(6), 673-689.

Contreras, M.T., Pasala, D.T.R. and Nagarajaiah, S. (2014), "Adaptive length SMA pendulum Smart tuned mass damper performance in the presence of real time primary system stiffness change", *Smart Struct. Syst.*, **13**(2), 219-233.

Dai, N.X. (2012), "Experimental and theoretial research on the smart isolation system using PZT and SMA complex friction damper", Ph.D. Dissertation , Hunan University, Changsha.

El-Attar, A., Saleh, A., El-Habbal, I., Zaghw, A.H. and Osman, A. (2008), "The use of SMA wire dampers to enhance the seismic performance of two historical Islamic minarets", *Smart Struct. Syst.*, **4**(2), 221-232.

Etedali, S., Sohrabi, M.R. and Tavakoli, S. (2013), "Optimal PD/PID control of smart base isolated buildings equipped with piezoelectric friction dampers", *Earthq. Eng. Eng. Vib.*, **12**(1), 39-54.

Liu, R.C., Jiao, L.C. and Du, H.F. (2005), "Clonal Strategy Algorithm Based on the Immune Memory", *J. Comput. Sci. Technol.*, **20**(5), 728-734.

Liu, Z.S., Wang, D.J., Hu, H.C. and Yu, M. (1994), "Measures of modal controllability and observability in vibration control of flexible Structures", *J. Guidance Control Dyn.*, **17**(6), 1377-1380.

Ok, S.Y., Song, J. and Park, K.S. (2008), "Optimal design of hysteretic dampers connecting adjacent structures using multi-objective genetic algorithm and stochastic linearization method", *Eng. Struct.*, **30**(5), 1240-1249.

Ozbulut, O.E. and Hurlebaus, S. (2010), "Fuzzy control of piezoelectric friction dampers for seismic protection of smart base isolated buildings", *Bull. Earthq. Eng.*, **8**(6), 1435-1455.

Sun, D.C., Song, Z. and Wang, D.J. (1999), "Hybrid control method of beams using two kinds of smart material", *Chinese J. Appl. Mech.*, **16**(4), 83-88.

Xu, B., He, J. and Dyke, S.J. (2015), "Model-free nonlinear restoring force identification for SMA dampers with double Chebyshev polynomials: approach and validation", *Nonlinear Dynam.*, **82**(3), 1507-1522.

Yan, G. and Zhou, L.L. (2006), "Integrated fuzzy logic and genetic algorithms for multi-objective control of structures using MR dampers", *J. Sound Vib.*, **296**(1-2), 368-382.

Yuvaraja, M. and Senthilkumar, M. (2013), "Comparative study on vibration characteristics of a flexible GFRP composite beam using SMA and PZT actuators", *Procedia Eng.*, **64**, 571-581.

Zhan, M., Wang, S.L., Zhu, X.Y. and Zhu, J.Q. (2014), "Semi-active optimization control of space truss model with piezoelectric friction damper", *J. Build. Struct.*, **35**(8), 50-56.

Zhao, D.H. and Li, H.N. (2011), "Seismic reduction tests of a model structure with piezoelectric friction damper", *J. Vib. Shock*, **30**(6), 272-276.

Zhou, X. and You, Z. (2015), "Theoretical analysis of superelastic SMA helical structures subjected to axial and torsional loads", *Smart Struct. Syst.*, **15**(5), 1271-1291.

CC